Chemically bonding BaTiO3 nanoparticles in highly filled polymer nanocomposites for greatly enhanced dielectric properties

Rui-Chao Chen, Quan-Ping Zhang, Kai Ke, Nan Sun, Wei-Di Xu, Dong-Liang Liu, Wenbin Yang, Yin-Tao Li, Yuan-Lin Zhou, Ming-Bo Yang, et al.

Chemically bonding $BaTiO_3$ nanoparticles in highly filled polymer nanocomposites for greatly enhanced dielectric properties

Rui-Chao Chen [a], Quan-Ping Zhang [a*], Kai Ke [b], Nan Sun [c], Wei-Di Xu [a], Dong-Liang Liu [a], Wenbin Yang [a], Yin-Tao Li [a], Yuan-Lin Zhou [a], Ming-Bo Yang [b], Jinkai Yuan [d*], Wei Yang [b*]

[a] State Key Laboratory of Environment-friendly Energy Materials, Southwest University of Science and Technology, Mianyang 621010, China

[b] College of Polymer Science and Engineering, State Key Laboratory of Polymer Materials Engineering, Sichuan University, Chengdu 610065, China

[c] Institute of Materials, China Academy of Engineering Physics, Jiangyou 621908, China

[d] Centre de Recherche Paul Pascal, CNRS, University of Bordeaux, UMR5031, 33600 Pessac, France

Corresponding authors: Quan-Ping Zhang; Jinkai Yuan; Wei Yang
E-mails: zhangqp@swust.edu.cn; jinkai.yuan@crpp.cnrs.fr; weiyang@scu.edu.cn

Abstract

Dielectric nanomaterials offer great promise for diverse technological applications such as capacitors, actuators, and sensors. Unfortunately, the exploitation of desirable dielectric properties in polymer nanocomposites is a great challenge due to lack of efficient routes to achieve uniform dispersion of nanoparticles and good compatibility of interfaces at high nanoparticle loadings. A dilemma between the nanofiller loading and dispersion as well as interfacial compatibility makes it impossible to fully exploit the intrinsic polarization of the nanoparticles. Herein, we break such dilemma and fabricate highly filled barium titanate/silicone rubber (BT/SR) nanocomposites through chemically bonding BT nanoparticles with SR by "thiol-ene click" and isostatic pressing techniques. BT loading varies from 88 wt% to 97 wt% without scarifying uniform dispersion quality and good interfacial adhesion with SR matrix. The 90 wt% BT nanocomposite shows an optimum dielectric constant as high as 55, while its loss tangent can be kept as low as 0.019 at 10^3 Hz. Meanwhile, it displays good stability of dielectric properties from room temperature up to 100 °C. In addition, the breakdown strength just decreases slightly compared to neat SR (97 MV/m) but is still beyond 75 MV/m. The present work provides a facile strategy towards superior dielectric polymer nanocomposites.

Keywords: Polymer nanocomposites; high nanofiller loading; dispersion; interface compatibility; dielectric properties.

Polymer-based high-dielectric-constant (high-*k*) materials have been explored for the extensive applications in modern electronic devices such as capacitors, actuators, sensors, and electromagnetic interference shielding due to their advantages of good processability, mechanical flexibility, light weight, low cost, and high breakdown strength [1-7]. Generally, it is challenging to use neat polymers to satisfy these needs because of their intrinsically low dielectric constant [8-12]. For instance, in spite of the high breakdown strength (730 MV/m), commercial benchmark polymer dielectric, biaxially oriented polypropylene (BOPP), shows a low dielectric constant (2.25) that is not favorable for its exploitation in electronic devices [13]. It is imperative to develop polymeric dielectrics that concurrently bear high dielectric constant and large breakdown strength.

It is widely accepted that incorporating high-*k* ceramics such as $BaTiO_3$ (BT) nanostructures into polymer matrices is one of the most effective ways to enhance the dielectric constant while profiting the high breakdown strength of polymers [14-19]. Several theoretical models have been proposed to describe the relationships between ceramic loading and dielectric constant of polymer nanocomposites, as shown in **Figure S1**. Emphases are respectively put on the shape, size, distance and connective pattern of ceramic nanoparticles in these models to predict the dielectric constant of the nanocomposites [20-23]. But the identical principle is that higher loading of ceramics gives rise to higher dielectric constant. This is because introducing high loading of ceramic nanoparticles into polymer matrices is potentially interesting to fully utilize the intrinsic polarization of ceramic nanoparticles and consequently

delivering ultrahigh dielectric constant.

Much work has demonstrated that enhanced dielectric constant can be achieved at high filler loading but at the expense of breakdown strength of polymer nanocomposites [23-26]. Actually, high loading of nanoparticles induces the formation of defects including nonuniform distribution of nanofillers, insufficient interfacial interactions between nanofillers and polymer matrices and occurrence of voids [27-29]. The charge separation at interfaces and strong electric field intensification usually lead to clear frequency dependence of dielectric properties and reduced breakdown strength [30-33]. In detail, large amount of space charges accumulate at the incompatible interfaces or voids and main channels of leakage current are easily introduced along the edges [34-36]. Moreover, the local electric field around the nanofillers can be several times larger than the applied electric field, which also causes the breakdown of the nanocomposites at the electric fields much weaker than the intrinsic breakdown strength of polymer matrices. Therefore, a huge challenge is making a compromise between enhancement of dielectric constant and reduction of breakdown strength at high filler loading to achieve good integrated dielectric properties of polymer nanocomposites.

To tackle this challenge, the key is to ensure uniform dispersion of nanofillers and good interfacial compatibility in the polymer nanocomposites at high filler loading [27-30, 37]. Considering the fact that the physiochemical properties of nanofillers and polymer matrices show a great disparity, and large surface-to-volume ratio of nanofillers [38-41]. Constructing sufficient reactive sites between nanofillers

and polymer chains is of great importance to intensify the interfacial interactions. So far, “grafting to” and “grafting from” strategies have been widely applied to connect nanofillers with polymer matrices through chemical bonds [42-45]. Typically, core-shell structures that organics or inorganics are coated on nanofillers, are further compounded with polymer matrices to form dielectric nanocomposites [46-48]. Unfortunately, the optimum filler loading corresponding to the good integrated dielectric properties has been determined by scanning within a relatively narrow filler content (0~50 vol.%). In fact, there is still great spaces to uniformly disperse more nanoparticles so that the upper limit of dielectric constant of polymer nanocomposites can be reached. This will allow for exploring the full potential of high-*k* nanoparticles to make best compromise between dielectric constant and breakdown strength and thus a superior integrated dielectric properties of polymer nanocomposites.

In this work, we present a facile means to make a highly filled polymer nanocomposite. A high pressure of 260 MPa is applied to obtain densely stacking of BT nanoparticles in highly filled BT/SR nanocomposites (BT loading varies from 88 wt% to 97 wt%) under an isostatic pressing condition. Uniform dispersion of nanofillers and good interfacial compatibility in the nanocomposites are achieved with a powerful and versatile “thiol-ene click” technique that shows striking advantages include high yields, rapid reaction rates, and regioselective reaction [49]. Interestingly, the 90 wt% BT/SR nanocomposite shows the largest dielectric constant of 54.9 at 10^3 Hz ever reported for polymer-based composites with 0 dimensional BT nanoparticles. Meanwhile, it still exhibits low dielectric loss (0.019) and a slight decrease in

breakdown strength in comparison with the neat SR. This work provides a new route to make full use of the intrinsic polarization of BT nanoparticles to enhance the dielectric constant of polymer nanocomposites.

Results and discussion

Fabrication of the highly filled BT/SR nanocomposites

As schematically depicted in **Figure 1a**, the fabrication of the highly filled BT/SR nanocomposites involves three steps. **Step 1**, BT nanoparticles are treated with hydrogen peroxide aqueous solution to form hydroxyl groups (BT-OH). Then BT nanoparticles are further modified with (3-mercaptopropyl) triethoxysilane (MPTES) [50]. The characteristic signals in X-ray photoelectron spectroscopy for silicon (Si2p at 101.7 eV) and sulphur (S2p at 163.55 eV) are detected, as shown in **Figure S2**. It confirms that a condensation reaction of triethoxysilane groups of MPTES with hydroxyl groups on the surface of BT nanoparticles occurs, which produces sufficient thiol groups on the surfaces of BT nanoparticles (BT-SH). **Step 2**, 1, 3, 5, 7-tetravinyl-1, 3, 5, 7-tetramethylcyclotetrasiloxan (V_4) as monomer and tetramethylammonium hydroxide (TMAH) as initiator are used to synthesize polymethylvinylsiloxane by anionic ring opening polymerization [51-52]. The polysiloxane shows a weight-average molecular weight (M_w) of 1.18×10^3 g/mol and a molecular distribution of 2.06, as represented in **Figure S3** and **Table S2**. **Step 3**, polymethylvinylsiloxane, BT-SH (88 wt%, 89 wt%, 90 wt%, 91 wt%, 93 wt%, 95 wt%, and 97 wt%), cross-linker 3, 6-Dioxa-1, 8-octanedithiol (DODT) and initiator 2,

2-dimethoxy-2-phenylacetophenone (DMPA) are compounded together with toluene.

Afterwards, conventional tableting technique is used to initially fabricate samples with 1.5 MPa of pressure. Then, an isostatic pressing technique is applied to further press the prefabricated samples with 260 MPa of ultrahigh pressure, as exhibited in **Figure 1b**. It should be pointed out the macroscopic size of the samples shrinks obviously after experiencing the ultrahigh pressure, as shown in **Figure 1c**. Namely, much densely stacking of BT nanoparticles was achieved. The sample thickness can vary from dozens of microns to macroscopic size scale, as shown in **Figure 1c** and **Figure 1d**, which can be tuned via tailoring the amount of the nanocomposites before tableting. It is of vital significance to their application in various electronic devices. Finally, BT nanoparticles are bonded with SR in the samples when the so-called “thiol-ene click” reaction is triggered at 80 °C [49]. TGA curves also depict the modification of BT nanoparticles and the fabrication of the highly filled nanocomposites with various filler loadings, as shown in **Figure S4**.

Increasing loading of functional fillers is an effective route to enhance dielectric constant of polymer composites [20-23]. However, it generally causes a great challenge to achieve uniform dispersion of nanofillers and good interfacial compatibility in nanocomposites, which are of vital importance to integrated dielectric performance. Here all BT nanoparticles are uniformly coated with a layer of SR and stacked densely in the 88 wt% BT/SR nanocomposites, as shown in **Figure 1e**. Namely, uniform dispersion of BT nanoparticles and good interfacial compatibility are clearly observed in such highly filled polymer nanocomposites. It is a great step

towards polymer nanocomposites with extremely high loading of nanofillers.

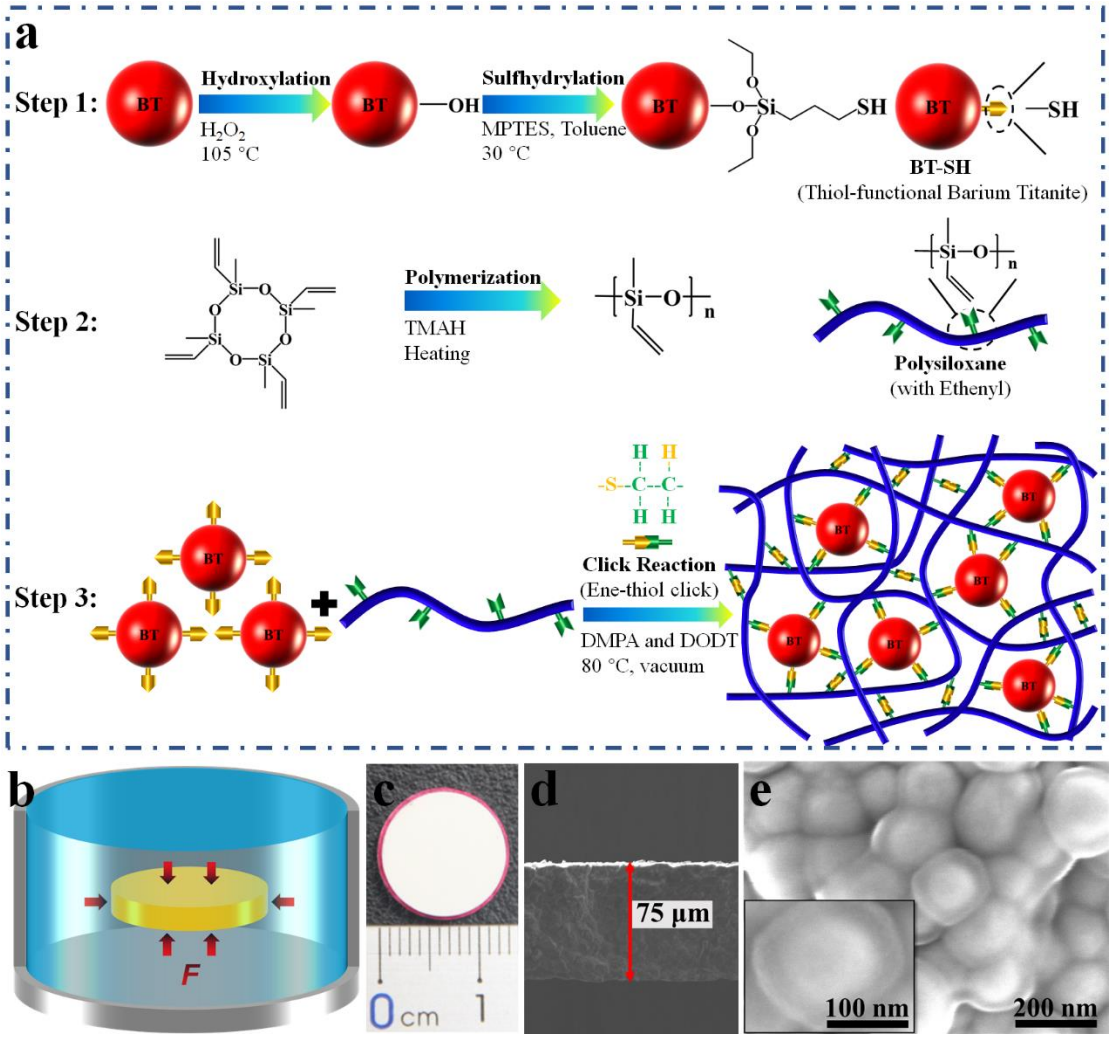

Figure 1. a: Schematic illustration of the fabrication process for the highly filled BT/SR nanocomposites. b: Sample subjecting to 260 MPa of ultrahigh pressure under isostatic pressing condition. c: Top view of the overlapping two samples, the upper sample with isostatic pressing while the bottom one marked red without. d: Cross section of the sample after isostatic pressing treatment. e: SEM image of the 88 wt% BT/SR nanocomposite.

Morphologies of the highly filled BT/SR nanocomposites

To determine the effects of extremely high loading of nanofiller on the microstructure, the morphologies of BT/SR nanocomposites are investigated in detail, as shown in **Figure 2**. **Figure 2a** and **Figure 2b** show that BT nanoparticles are

coated and meanwhile bonded with a thin SR layer in the nanocomposite with 97 wt% BT. Namely, desirable uniform dispersion of BT nanoparticles and good interfacial compatibility are achieved simultaneously. This is because that all the thiols (-SH) on the surfaces of BT nanoparticles can react with the enough enes (-CH=CH_2) in the polymethylvinylsiloxane chains via typical “thiol-ene click” [49]. However, a new issue arises, that is unfavorable voids in the nanocomposites. The voids are detrimental for achieving high dielectric constant, low loss and large breakdown strength in polymer nanocomposites [17-19]. Note that voids gradually diminish with decreasing the BT loading. They are difficult to be found in the nanocomposites with 88 wt% BT, as shown in **Figure 2a, Figure 2d** and **Figure 2g**. This is due to the fact that the voids are gradually replaced by SR with increasing the amount of the polymer. Moreover, the thickness of SR layer on BT nanoparticles becomes thicker at the lower BT loadings and much more indistinct interfaces can be found at 88 wt% BT loading, as shown in **Figure 2b, Figure 2e** and **Figure 2h**. BT nanoparticles connect with SR layer rather than direct contact with each other and few voids are observed between BT nanoparticles, as shown in **Figure 2j** and **Figure 2k**. Meanwhile, **Figure 1c** exhibits the applied 260 MPa of high pressure distinctly shrinks the size of sample. Namely, it makes the densely stacking of BT nanoparticles in a way much similar to the face-centered cubic (FCC) pattern and extra SR filling the voids during isostatic pressing. **Figure 2c**, **Figure 2f** and **Figure 2i** depict the stacking pattern of BT nanoparticles and declining volume of voids in the nanocomposites with decreasing BT loading. The polymethylvinylsiloxane chains are anchored on the surface of BT

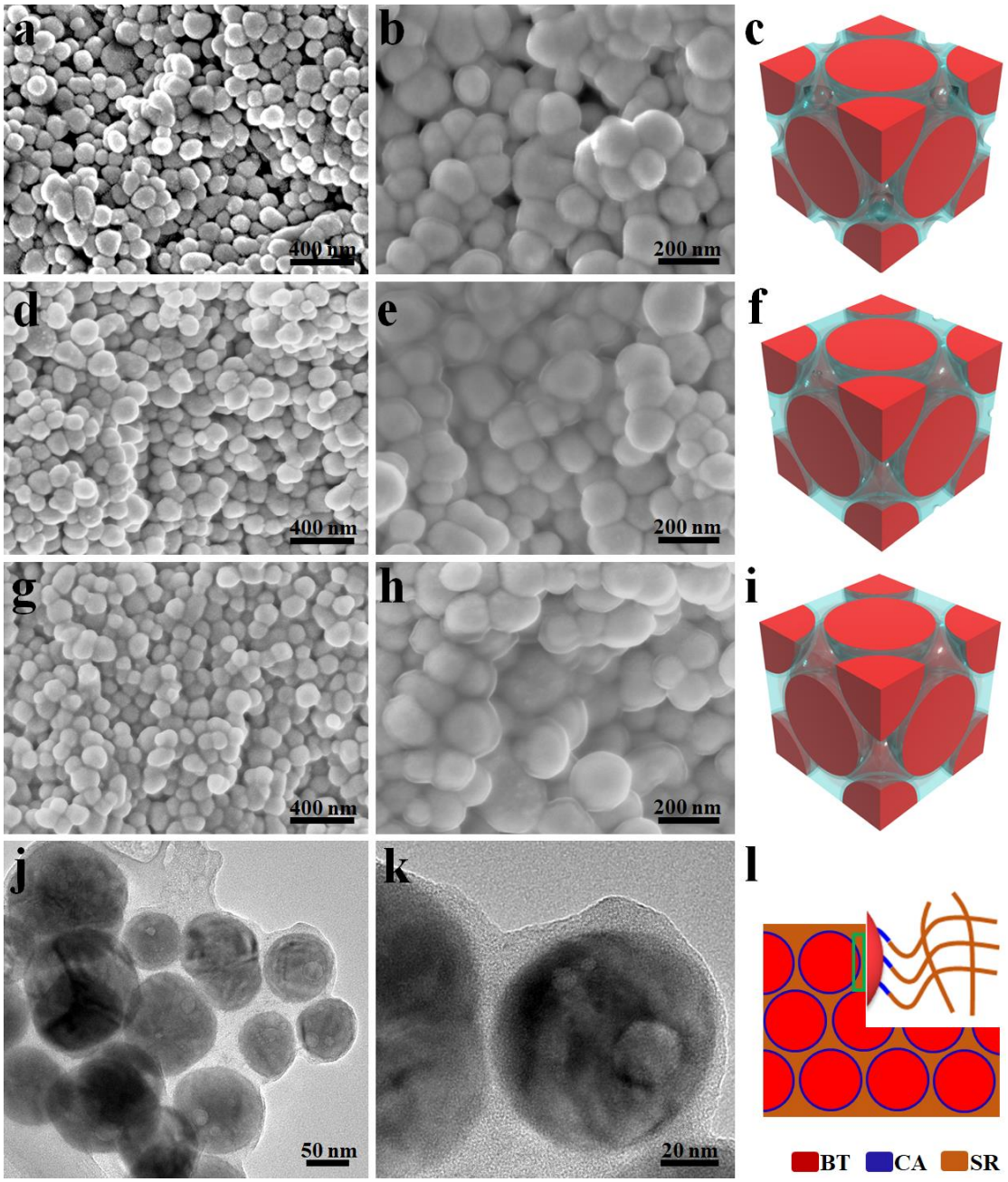

Figure 2. Morphologies of BT/SR nanocomposites with various BT loadings. SEM images of the nanocomposites with (a, b) 97 wt% BT, (d, e) 90 wt% BT and (g, h) 88 wt% BT. TEM images of the nanocomposites with (j, k) 88 wt% BT. Packing pattern of BT nanoparticles (c) 97 wt% BT, (f) 90 wt% BT and (i) 88 wt% BT in the nanocomposites. (l) Topological chains of SR on the surfaces of BT at the interfaces. CA represents the silane coupling agents.

nanoparticles with covalent bonds, as depicted in **Figure** 2**l**. Meanwhile, the polysiloxane can be crosslinked into SR coating on BT nanoparticles. These results indicate that SR is first coated on the surface of BT nanoparticles and then the extra

SR is used for filling the voids between the densely packed BT nanoparticles. Importantly, this unique fabrication strategy provides an effective means to achieve a series of desirable features such as uniform dispersion of nanofillers, good interfacial compatibility as well as avoidance of voids in highly filled polymer nanocomposites.

Dielectric properties of the highly filled BT/SR nanocomposites

Figure 3 shows the dielectric properties of BT/SR nanocomposites with various BT loadings. Dielectric constant and dielectric loss of the highly filled polymer nanocomposites display a negligible dependence on the frequency from 10^3 to 10^7 Hz, as shown in **Figure 3a** and **Figure 3b**. Usually, Effective-Medium Theory (EMT) model is utilized to predict the dielectric constant of polymer composites filled with 0 dimensional fillers [22]. Unexpectedly, the variation trend for the dielectric constants of the nanocomposites with increasing the loading of BT nanoparticles deviates from the model, as displayed in **Figure S5b**. It can be seen the dielectric constant first increases and then decreases with increasing BT loading, as depicted in **Figure 3c**. All the nanocomposites exhibit significant increases of dielectric constants in comparison with neat SR. Particularly, the 90 wt% BT/SR nanocomposite shows a dielectric constant of 54.9 at 10^3 Hz, which is about 22 times larger than that of neat SR. The nanocomposites with even higher BT loadings fail to display even larger values of dielectric constant. Furthermore, dielectric loss increases slowly with increasing BT loading, as depicted in **Figure 3d**. It increases from 0.0121 for the neat SR, 0.0188 for the 90 wt% BT/SR nanocomposites and finally to 0.0215 for the 97 wt% BT/SR nanocomposites.

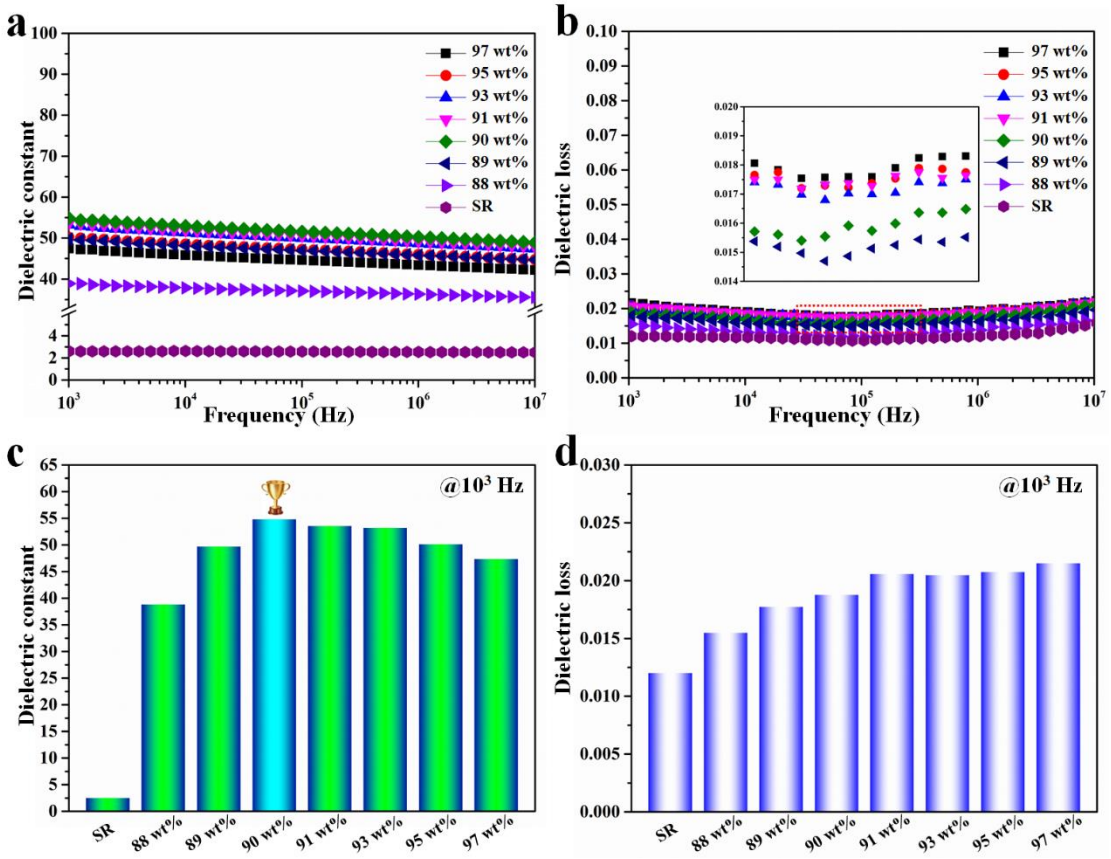

Figure 3. Frequency dependence of dielectric constants (a) and dielectric losses (b) of the high-filled BT/SR nanocomposites at room temperature. Comparison of the dielectric constants (c) and dielectric losses (d) of the nanocomposites with various BT loadings.

Interfacial polarization is one of the key factors directing the dielectric performance of polymer nanocomposites [17-19]. It is believed that dielectric constant of polymer nanocomposites usually decreases with frequency [31]. This is due to the fact interfacial polarization has a long relaxation time. When the spinning of interfacial polarization fails to keep up with the frequency of the applied electric field, the dielectric constants decrease at higher frequency. Regarding the highly filled BT/SR nanocomposites, the SR layer is fully anchored onto the surfaces of BT nanoparticles via “thiol-ene click”. The SR layer not only plays the roles of interface but also chemically bonds BT nanoparticles together for fabricating the final polymer nanocomposites. **Figure 2** suggests that enough “thiol-ene click” reactions occur due

to the rich "-CH=CH_2" in the polymethylvinylsiloxane chains and "-SH" on the surfaces of BT nanoparticles. Namely, a great number of "click" reaction contributes to good interfacial compatibility in the highly filled polymer nanocomposites. Accordingly, the negligible frequency dependence of dielectric properties for the polymer nanocomposites can be explained as follows. The movement of the polymer segments is confined greatly. Most of the polysiloxane chains are anchored on the surfaces of BT nanoparticles. That is, the interfaces in the polymer nanocomposites are compacted, as shown in **Figure 2k**. In this case, the space charge polarization at the interfaces, which is an important factor causing the frequency dependence of dielectric properties, is suppressed largely. Besides, the solution compounding facilitates the uniform dispersion of BT nanoparticles in the polysiloxane [53]. Then, uniform dispersion of BT nanoparticles is chemically bonded together with SR after "thiol-ene click". These results prove that the excellent dielectric properties of the highly filled nanocomposites are attributed to the desirable microstructures including uniform dispersion of BT nanoparticles, good interfacial compatibility.

For the highly filled polymer nanocomposites, an unexpected BT loading dependence of dielectric constant is also observed. The dielectric constant of the polymer nanocomposites gradually increases until 90 wt % BT loading while it turns reverse change with further increase in BT loading. According to some theoretical models [21-23], dielectric constant of polymer composites is in direct proportion to filler loading. But in this case, obvious voids can be seen at the 97 wt% BT/SR nanocomposites, as shown in **Figure 2a**. At the applied ultrahigh pressure, BT

nanoparticles coated with SR are stacked closely while too low loading of SR fails to fully fill the space between BT nanoparticles, leading to the formation voids, as depicted in **Figure 2c**. The voids are equal to introducing a third phase (air) into the polymer nanocomposites. The so-called third phase displays much lower dielectric constant ($k \approx 1$) than BT and SR. Then, extremely high loading of BT nanoparticles means there is nonnegligible voids in the nanocomposites, which causes the reduction of dielectric constants according to the theoretical models. Meanwhile, considerable space charge polarization occurs in this case, which also leads to high dielectric loss, as shown in **Figure 3c** and **Figure 3d**. Note that the volume fraction of voids decreases with decreasing BT loading and few voids are observed at 88 wt% BT/SR nanocomposites, as depicted in **Figure 2c, Figure 2f** and **Figure 2i**.

To better understand the dielectric behavior, the volume fraction of voids in the highly filled polymer nanocomposites is calculated, as shown in **Figure S5**. As discussed above, BT nanoparticles stack densely, which is supposed to be an ideal condition with the fixed size of particles and FCC stacking pattern, as depicted in **Figure 2c, Figure 2f** and **Figure 2i**. **Table S3** lists the key parameters for the calculation and **Table S4** lists the calculated volume fraction of voids in the polymer nanocomposites with various BT loadings. The results show the largest volume fraction of voids exists in the 97 wt% BT/SR nanocomposite and the volume fraction of voids gradually decreases and even disappears in the nanocomposites with decreasing BT loading. The thickness of SR layer coated on BT nanoparticles is another factor to the critical BT loading for the occurrence of voids. This is because

SR is used not only for coating BT nanoparticles but also for filling the space between BT nanoparticles. Larger thicknesses of SR layer mean higher volume fraction of voids between BT nanoparticles. **Figure 2** shows the thickness of SR layer coated on BT nanoparticles is usually below 3 nm. Namely, 88 wt% BT loading can lead to few voids in the nanocomposites in that the mass fraction is lower than the critical value (89.28 wt%). Similarly, 90 wt% BT loading tends to cause just a few voids because it is very close to the critical value. In fact, BT nanoparticles exhibit a wide size distribution, as shown in **Figure 2j**. The nanoparticles with smaller sizes incline to be pushed into the space between larger particles under the ultrahigh pressure [27], which further increases the critical value.

Figure 4 shows the stability of dielectric properties of 88 wt% and 90 wt% BT/SR nanocomposites from room temperature up to 100 °C. The 88 wt% BT/SR nanocomposite represents a mild increase of dielectric response, especially dielectric constants, as shown in **Figure 4 a** and **Figure 4b.** The dielectric stability of the nanocomposites indicates it is potential for the application of electronic devices. However, the 90 wt% BT/SR nanocomposite displays a higher increase in the dielectric responses, as shown in **Figure 4c** and **Figure 4d**. Charge carriers prefer to aggregate at the voids in the highly filled polymer nanocomposites. The potential barrier at relatively low temperature could prevent the charge carriers from shifting. Enhanced thermal motion at the increased temperature facilitates the migration of charge carriers that results in the enhancement of dielectric constant and dielectric loss. These results further demonstrate that much less voids tend to be formed in the

88 wt% BT/SR nanocomposite than the polymer composites with higher BT loading.

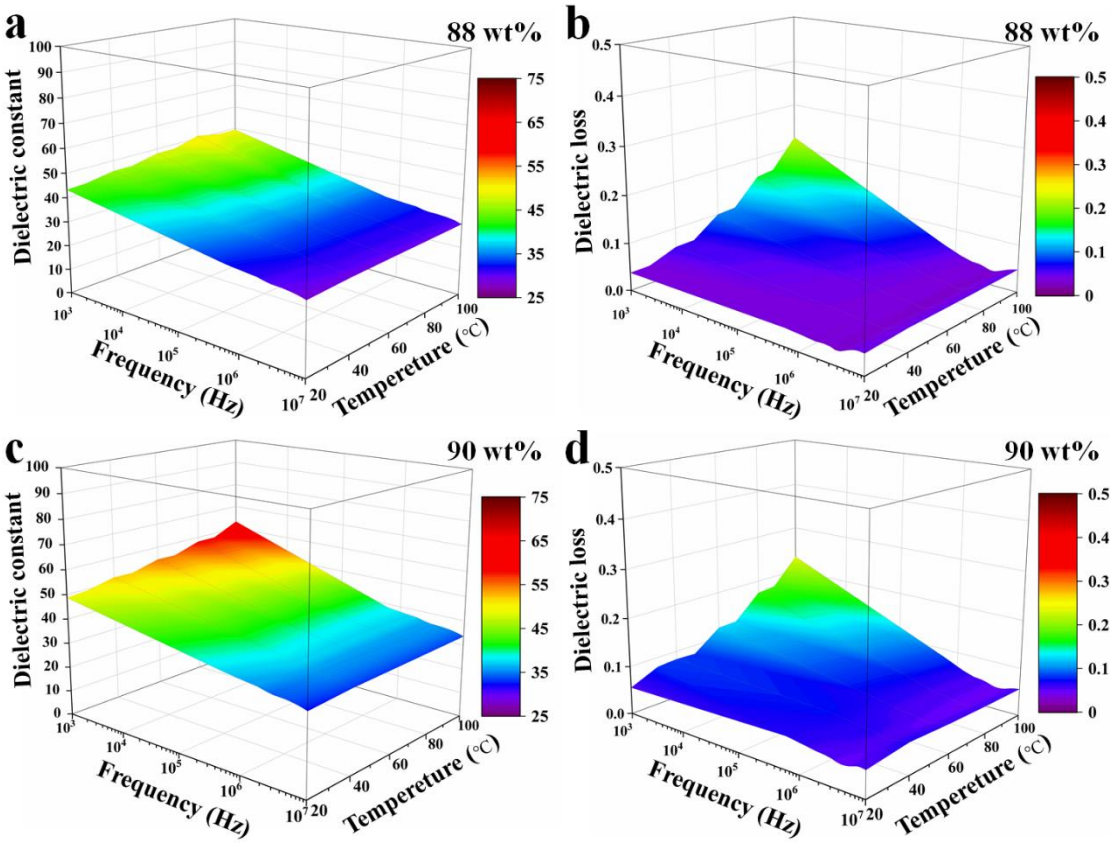

Figure 4 Temperature dependence of dielectric properties of BT/SR nanocomposites.

Breakdown strength of the highly filled BT/SR nanocomposites

Breakdown strength is another key for envaluating the dielectric properties of polymer nanocomposites. The failure probability of neat SR, BT/SR nanocomposites with 88 wt% and 90 wt% BT loading is investigated according to the Weibull distribution function.

$$P(E) = 1 - e^{-(E/E_b)^{\beta}} \qquad (2)$$

where $P(E)$ is the cumulative failure probability, E is the measured breakdown strength, E_b is the Weibull breakdown strength with 63.2% probability to breakdown, and β is the shape parameter or the slope of the derived logarithm equation as

$$\ln[-\ln(1-P_{(E)}] = \beta \ln E - \beta \ln E_b \qquad (3)$$

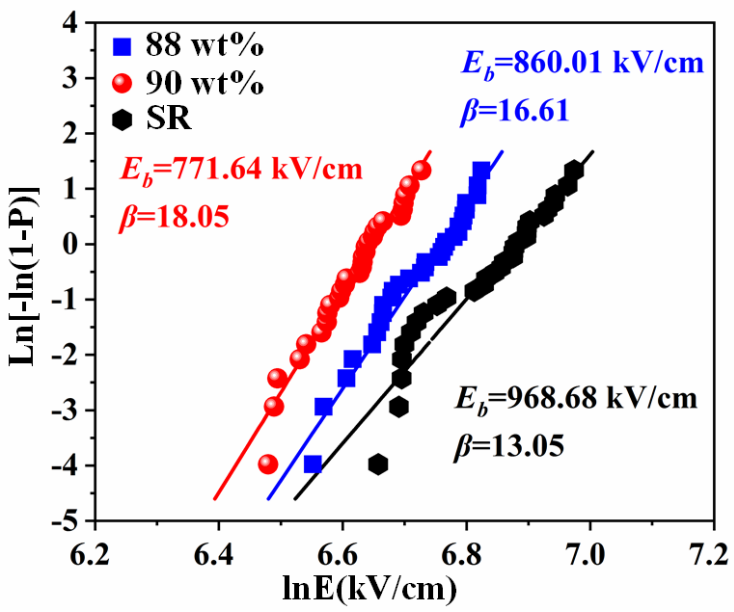

Figure 5. Cumulative failure probability distribution of the neat SR, 88 wt% and 90 wt% BT/SR composites.

As depicted in **Figure 5**, the E_b of neat SR is 968.68 kV/cm. A slight decrease of breakdown strength to 860.01 kV/cm and 771.64 kV/cm is observed for the nanocomposites with 88 wt% and 90 wt% BT loading, respectively. It should be pointed out the modulus of polymer matrix plays an important role in the breakdown strength of polymer nanocomposites [54]. The relatively low modulus of the silicone rubber causes the unremarkable breakdown strength of the highly filled polymer nanocomposites. In addition, it is believed that defects in nanocomposites such as voids facilitate the propagation of electrical treeing, which causes lower dielectric breakdown strength. That is, less defects exist in the 88 wt% BT/SR nanocomposite than the nanocomposites with higher BT loading. Importantly, the slight decrease in the breakdown strength of both nanocomposites indicates that the unique fabrication route contributes to avoiding the formation of numerous defects in the highly filled polymer nanocomposites. Besides, the β value increases from 13.05 for neat SR, to

16.61 for the 88 wt% BT/SR nanocomposite, and to 18.65 for the 90 wt% BT/SR nanocomposite. The narrow distribution of breakdown strength indicates that the polymer nanocomposites possess excellent dielectric reliability.

Comparison of dielectric properties of highly filled polymer nanocomposites

To characterize the integrated dielectric properties more directly, a radar chart is depicted in **Figure 6** for the 90 wt% BT/SR nanocomposite and the representative polymer nanocomposites with 0 dimensional BT nanoparticles [30, 55-56]. Since the dielectric properties of polymer nanocomposites are also related to the matrix, the values of $\varepsilon_{eff}/\varepsilon_m$ and E_b/E_m are used for comparison, which are detailed and listed in **Table S5**. It is clear BT/SR nanocomposite with extremely high BT loading in this work manifests much better $\varepsilon_{eff}/\varepsilon_m$ of about 21.85 in comparison with other polymer nanocomposites at 10^3 Hz of frequency. It is believed extremely high BT loading usually leads to negative effects on the dielectric loss and breakdown strength due to the probable defects in highly filled polymer nanocomposites. Interestingly, it still exhibits low dielectric loss and high breakdown strength, which are comparable to the other polymer nanocomposites with the excellent properties. Namely, less internal heating and long lifetime are hopefully to be realized. These results suggest that BT/SR nanocomposites prepared in this unique route possess greatly integrated dielectric properties.

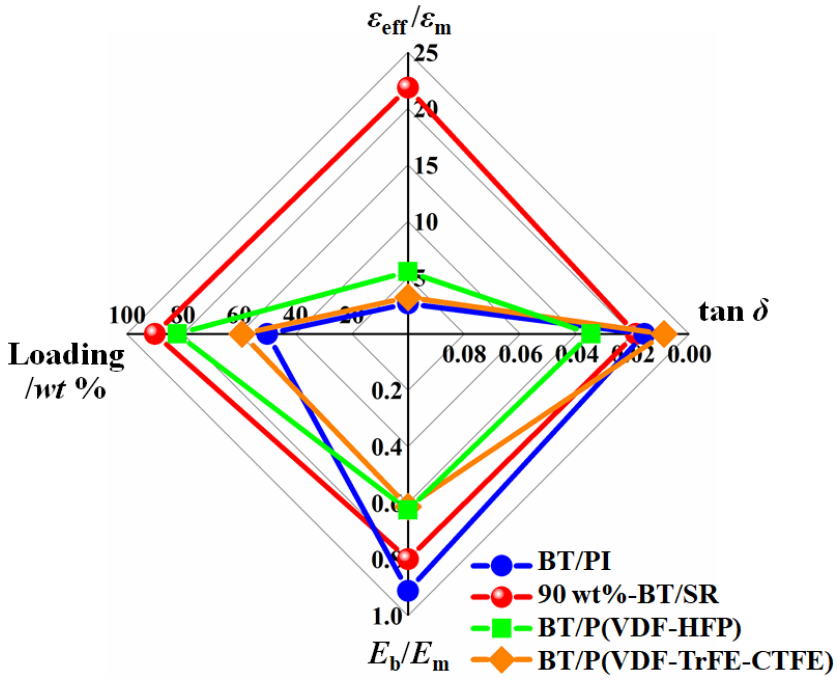

Figure 6 Comparison of the dielectric properties of polymer nanocomposites with 0 dimensional BT nanoparticles, BT/PI [55], BT/P(VDF-HFP) [30], and BT/P(VDF-TrFE-CTFE) [56].

Conclusions

Highly filled BT/SR nanocomposites with desired morphologies that include uniform dispersion of BT nanoparticles, good interfacial compatibility and few voids are obtained through typical "thiol-ene click" and isostatic pressing with greatly high pressure. The dielectric constant of the nanocomposites first enhances and then reduces with increasing BT loading from 88% to 97wt%. Importantly, the 90 wt% BT/SR nanocomposite shows the largest dielectric constant (54.9 at 10^3 Hz) in polymer nanocomposites with 0 dimensional BT as fillers ever reported. Meanwhile, the dielectric loss is immensely suppressed to about 0.019. Meanwhile, it displays good dielectric stability from room temperature to 100 °C. Besides, a slight decrease in breakdown strength with the neat SR is maintained. As a result, this work provides

an effective strategy to fabricate highly filled polymer nanocomposites with excellently integrated dielectric properties that are highly potential to be used for diverse electronic devices.

Experimental section

Surface modification of $BaTiO_3$ (BT) nanoparticles: BT nanoparticles (HBT-010, $\bar{d}$ ≈100nm, cubic crystal, as shown in **Figure S6**) were purchased from Shandong Sinocera Functional Material Company. A mixture with 20 g BT nanoparticles and 200 mL H_2O_2 solution (30% mass fraction) was first ultrasonically treated for 30 mins. To initiate hydroxylation surface treatment of BT nanoparticles, the mixture was heated at 105 °C for 9h under intense stirring with reflux. After that, the mixture is successively subject to centrifugation, washing with deionized water and ethanol repeatedly, and drying treatment. Second, adding the dried product into toluene (200mL) was ultrasonically treated again. Then, (3-Mercaptopropyl) triethoxysilane (Shanghai Aladdin Bio-Chem Technology Co., LTD) was introduced into the mixture and stirred at 30 °C under N_2 atmosphere for 48h. After that, the mixture was successively subject to centrifugation, washing with toluene repeatedly, and vacuum drying treatment at room temperature. Finally, sulfhydrylated $BaTiO_3$ (BT-SH) nanoparticles were achieved.

Synthesis of PMVSO: 1,3,5,7-tetravinyl-1,3,5,7-tetramethylcyclotetrasiloxane (V_4, Guangdong Weng Jiang Reagent Co., Ltd) as the monomer and tetramethylammonium hydroxide (TMAH) as the initiator were applied to synthesize

polymethylvinylsiloxane via anionic ring opening polymerization.

Preparation of $BaTiO_3$/Silicone Rubber (BT/SR) composites: Functional nanoparticles (BT-SH), polysiloxane (polymethylvinylsiloxane), cross-linker (3, 6-Dioxa-1, 8-octanedithioln, Shanghai Aladdin), and initiator (2, 2-Dimethoxy-2-phenylacetophenone, Shanghai Aladdin) were mixed with toluene under intense stirring. The toluene was then removed under vacuum at room temperature. After that, the white power was put into a 13 mm diameter mold and initially pressed at 1.5 MPa. After that the pill was isostatically pressed at 260 MPa for 5 mins. Finally, the pressed pill was treated under vacuum at 80°C for 24h and the BT/SR nanocomposite was obtained.

Structure characterization and performance evaluation: Scanning electron microscope (SEM, JSM-7610F, JEOL, Japan) and transmission electron microscope (TEM, Tecani F20, FEI Company, Neatherlands) were applied to examine the morphology of BT and BT/SR composites. Thermal gravimetric analyzer (TGA, SDT Q600, TA Instruments, USA) was applied to determine the relation of weight loss and temperature at a rate of 20 °C/min from 100 °C to 800 °C under N_2 atmosphere. X-Ray diffractometer (XRD, DMAX1400, Rigaku Corporation, Japan) in Cu $K_{\alpha 1}$ radiation, λ = 1.5406 Å with a range from 3° to 80° was used to investigate the crystal phase of BT nanoparticles. The molecular parameter of PMVSO was determined by gel permeation chromatography (GPC, PL-GPC220, Polymer Laboratories Ltd, the UK). The BT/SR samples were sputtered with circular gold electrode with 8 mm diagram on both sides for dielectric performance measurements. The dielectric properties at room temperature were evaluated using a precision impedance analyzer (4294A, Agilent Technologies Inc., USA) at a range from 10^3 Hz to 10^7 Hz. The

dielectric properties with an interval of 20 °C from room temperature up to 100 °C at a range from 10^3 Hz to 10^7 Hz were tested using a broadband dielectric analyzer (Concept-50, Novocontrol GmbH, Germany). The electric breakdown strength was determined with a withstanding voltage tester (DDJ-50KV, Beijing Guancejingdian Equipment Ltd, China) with an increasing voltage of 200 V/s.

Author contribution statement

Rui-Chao Chen performed the main experiments of the work.

Quan-Ping Zhang designed the experiments and prepared the manuscript.

Kai Ke and Nan Sun conducted the dielectric tests.

Wei-Di Xu synthesized polysiloxane.

Dong-Liang Liu did TEM observation.

Wenbin Yang, Yin-Tao Li, Yuan-Lin Zhou and Ming-Bo Yang took part in the discussion of structure and performance.

Jinkai Yuan and Wei Yang took part in the design of the experiments and revised the manuscript.

Conflicts of interest

The authors declare no conflicts of interest.

Acknowledgements

The authors would like to thank Professor Lei Zhu at Case Western Reserve University for the discussion on the relationship of structures and properties of polymer nanocomposites. This work was supported by the National Natural Science Foundation of China (11747042, 51873126 and 51422305), Science and

Technology Development Foundation of China Academy of Engineering Physics (xk201701), Sichuan Science and Technology Program (2019YJ0445), Project of State Key Laboratory of Environment-friendly Energy Materials (17FKSY0105).

References

1. Q. Li, L. Chen, M. R. Gadinski, S. Zhang, G. Zhang, H. Li, A. Haque, L. Q. Chen, T. Jackson and Q. Wang, *Nature*, 2015, **523**, 576-580.
2. S. Luo, Y. Shen, S. Yu, Y. Wan, W. H. Liao, R. Sun and C. P. Wong, *Energy Environ. Sci.*, 2017, **10**, 137-146.
3. F. Torres-Canas, J. Yuan, I. Ly, W. Neri, A. Colin and P. Poulin, *Adv. Funct. Mater.*, 2019, **29**, 1901884.
4. B. Fan, M. Zhou, C. Zhang, D. Hea and J. Bai, *Prog. Polym. Sci.*, 2019, **97**, 101143.
5. X. Xie, C. Yang, X. Qi, J. Yang, Z. Zhou, Y. Wang, *Chem. Eng. J.* 2019, **366**, 378-389.
6. J. -Y. Kim, E. K. Lee, J. Jung, D. -W. Lee, Y. Yun, J. W. Chung, J.-I. Park and J. -J. Kim, *J. Mater. Chem. C*, 2019, **7**, 5821-5829.
7. N. A. Shepelin, A. M. Glushenkov, V. C. Lussini, P. J. Fox, G. W. Dicinoski, J. G. Shapter and A. V. Ellis, *Energy Environ. Sci.*, 2019, **12**, 1143-1176.
8. Y. Shen, X. Zhang, M. Li, Y. Lin and C.-W. Nan, *Natl. Sci. Rev.*, 2017, **4**, 23-25.
9. Z. Yao, Z. Song, H. Hao, Z. Yu, M. Cao, S. Zhang, M. T. Lanagan and H. Liu, *Adv. Mater.*, 2017, **29**, 1601727.
10. B. Chu, X. Zhou, K. Ren, B. Neese, M. Lin, Q. Wang, F. Bauer and Q.M. Zhang, *Science*, 2006, **313**, 334-336.
11. Q.-P. Zhang, W.-F. Zhu, D.-M. Liang, X.-L. Wu, R.-C. Chen, N. Sun, Y.-T. Li and Y.-L. Zhou, *Appl. Surf. Sci.*, 2019, **487**, 77-81.
12. Z.-H. Shen, J.-J. Wang, Y. Lin, C.-W. Nan, L.-Q. Chen and Y. Shen, *Adv. Mater.*, 2018, **30**, 1704380.
13. Z. Zhang, D. H. Wang, M. H. Litt, L.-S. Tan and L. Zhu, *Angew. Chem. Int. Ed.*,

2018, **57**, 1528-1531.

14. H. Luo, X. Zhou, R. Guo, X. Yuan, H. Chen, I. Abrahams and D. Zhang, *Mater. Adv.*, 2020, **1**, 14-19.
15. R. Guo, J. I. Roscow, C. R. Bowen, H. Luo, Y. Huang, Y. Ma, K. Zhou and D. Zhang, *J. Mater. Chem. A*, 2020, **8**, 3135-3144.
16. D. Caruntu, B. Kavey, S. Paul, A. C. Bas, A. Rotaru and G. Caruntu, *CrystEngComm*, 2020, **22**, 1261-1272.
17. Y. Shen, Y. Lin and Q.M. Zhang, *MRS Bulletin*, 2015, **40**, 753-759.
18. Prateek, V. K. Thakur and R. K. Gupta, *Chem. Rev.*, 2016, **116**, 4260-4317.
19. B. Jiang, J. Iocozzia, L. Zhao, H. Zhang, Y.-W. Harn, Y. Chen and Z. Lin, *Chem. Soc. Rev.*, 2019, **48**, 1194-1228.
20. H. Frolich, Theory of Dielectrics, Oxford: Clarendon Press 1949.
21. G. Catalan, D. O' Neill, R. M. Bowman and J. M. Gregg, *Appl. Phys. Lett.*, 2000, **77**, 3078-3080.
22. Y. Rao, J. Qu, T. Marinis and C. P. Wong, *IEEE T. Compon. Pack. T.*, 2000, **23**, 680-683.
23. Z.-M. Dang, J.-K. Yuan, J.-W. Zha, T. Zhou, S.-T. Li and G.-H. Hu, *Prog, Mater, Sci.*, 2012, **57**, 660-723.
24. J. Y. Li, L. Zhang and S. Ducharme, *Appl. Phys. Lett.*, 2007, **90**, 132901.
25. Y. Wang, J. Cui, Q. Yuan, Y. Niu, Y. Bai and H. Wang, *Adv. Mater.*, 2015, **27**, 6658-6663.
26. L. Yao, D. Wang, P. Hu, B.-Z. Han and Z.-M. Dang, *Adv. Mater. Interfaces*, 2016, **3**, 1600016.
27. M. M. Rueda, M.-C. Auscher, R. Fulchiron, T. Périéc, G. Martinb, P. Sonntag and P. Cassagnau, *Prog. Polym. Sci.*, 2017, **66**, 22-53.
28. Y. Song and Q. Zheng, *Prog. Mater. Sci.*, 2016, **84**, 1-58.
29. Y. Feng, Q. Deng, C. Peng, J. Hu, Y. Li, Q. Wu and Z. Xu, *J. Mater. Chem. C*, 2018, **6**, 13283-13292.
30. P. Kim, N. M. Doss, J. P. Tillotson, P. J. Hotchkiss, M.-J. Pan, S. R. Marder, J. Li,

J. P. Calame and J. W. Perry, *ACS Nano*, 2009, **3**, 2581-2592.

31. L. Zhu, *J. Phys. Chem. Lett.*, 2014, **5**, 3677-3687.

32. L. Yao, Z. Pan, J. Zhai and H. Chen, *Nanoscale*, 2017, **9**, 4255-4264.

33. T. J. Lewis, *IEEE Trans. Dielectr. Electr. Insul.*, 2004, **11**, 739-753.

34. O. Levy and D. Stroud, *Phys. Rev. B*, 1997, **56**, 8035.

35. E. Baer and L. Zhu, *Macromolecules*, 2017, **50**, 2239-2256.

36. Z. Pan, L. Yao, J. Zhai, X. Yao and H. Chen, *Adv. Mater.*, 2018, **30**, 1705662.

37. G. Zhang, D. Brannum, D. Dong, L. Tang, E. Allahyarov, S. Tang, K. Kodweis, J.-K. Lee and L. Zhu, *Chem. Mater.*, 2016, **28**, 4646-4660.

38. H. Luo, X. Zhou, C. Ellingford, Y. Zhang, S. Chen, K. Zhou, D. Zhang, C. R. Bowen and C. Wan, *Chem. Soc. Rev.* 2019, **48**, 4424-4465.

39. S. Liu, B. Shen, H. Hao and J. Zhai, *J. Mater. Chem. C*, 2019, **7**, 15118-15135.

40. Y. Li, Y. Zhou, Y. Zhu, S. Cheng, C. Yuan, J. Hu, J. He and Q. Li, *J. Mater. Chem. A*, 2020, **8**, 6576-6585.

41. W. Li, Z. Song, J. Zhong, J. Qian, Z. Tan, X. Wu, H. Chu, W. Nie and X. Ran, *J. Mater. Chem. C*, 2019, **7**, 10371-10378.

42. H. Luo, C. Ma, X. Zhou, S. Chen and D. Zhang, *Macromolecules*, 2017, **50**, 5132-5137.

43. K. Yang, X. Huang, M. Zhu, L. Xie, T. Tanaka and P. Jiang, *ACS Appl. Mater. Interfaces*, 2014, **6**, 1812-1822.

44. Y. Kim, M. Kathaperumal, V. W. Chen, Y. Park, C. Fuentes-Hernandez, M.-J. Pan, B. Kippelen and J. W. Perry, *Adv. Energy Mater.*, 2015, **5**, 1500767.

45. H. Ye, X. Zhang, C. Xu, B. Han and L. Xu, *J. Mater. Chem. C*, 2018, **6**, 11144-11155.

46. M. Guo, J. Jiang, Z. Shen, Y. Lin, C.-W. Nan and Y. Shen, *Mater. Today*, 2019, **29**, 49-67.

47. F. E. Bouharras, M. Raihane, G. Silly, C. Totee and B, Ameduri, *Polym. Chem.*, 2019, **10**, 891-904.

48. Y. Qiao, X. Yin, L. Wang, M. S. Islam, B. C. Benicewicz, H. J. Ploehn and C.

Tang, *Macromolecules*, 2015, **48**, 8998-9006.

49. C. E. Hoyle and C. N. Bowman, *Angew. Chem. Int. Ed.*, 2010, **49**, 1540-1573.
50. L. G. Bach, M. R. Islam, J. T. Kim, S. Y. Seo and K. T. Lim, *Appl. Sur. Sci.*, 2012, **258**, 2959-2966.
51. Q.-P. Zhang, J.-H. Liu, H.-D. Liu, F. Jia, Y.-L. Zhou and J. Zheng, *Appl. Phys. Lett.*, 2017, **111**, 152901.
52. S. J. Dünki, Y. S. Ko, F. A. Nüesch, and D. M. Opris, *Adv. Funct. Mater.*, 2015, **25**, 2467-2475.
53. Y.-C. Lu, J. Yu, J. Huang, S. Yu, X. Zeng, R. Sun and C.-P. Wong, *Appl. Phys. Lett.*, 2019, **114**, 233901.
54. Z.-H. Shen, J.-J. Wang, J.-Y. Jiang, S. X. Huang, Y.-H. Lin, C.-W. Nan, L.-Q. Chen, and Y. Shen, *Nat. Commun.*, 2019, 10, 1843.
55. J. Ru, D. Min, M. Lanagan, S. Li, G. Chen, *Appl. Phys. Lett.* 2019, 115, 213901.
56. S. Chen, X. Lv, X. Han, H. Luo, C.R. Bowen and D. Zhang, *Polym. Chem*., 2018, **9**, 548-557.

Graphical Abstract

Extremely high loading of $BaTiO_3$ nanoparticles are chemically bonded with silicone rubber via “thiol-ene click”, leading to superior dielectric properties.